Resilient Cities and Structures 4 (2025) 143–157

Contents lists available at ScienceDirect

Resilient Cities and Structures

journal homepage: www.elsevier.com/locate/rcns

Full Length Article

Reducing the magnitude and variability of seismic-induced acceleration and force responses in steel buildings with controlled rocking base mechanism and force-limiting connections

Georgios Tsampras [a,*], Richard Sause [b]

[a] Department of Structural Engineering, University of California San Diego, USA
[b] Department of Civil and Environmental Engineering, Lehigh University, USA

ARTICLE INFO

Keywords:
Force-limiting connections
Rocking
Self-centering
Steel concentrically braced frames
Reduced variability
Higher-mode effects

ABSTRACT

This study numerically investigates the seismic response of a nine-story self-centering concentrically braced frame building incorporating force-limiting connections between the floor system and the lateral force-resisting system. Nonlinear earthquake simulations are conducted under design basis earthquake ground motions, and the results are compared against a baseline model with rigid-elastic connections. The study discusses connection design considerations and evaluates the effectiveness of force-limiting connections in mitigating higher-mode effects. The findings show that force-limiting connections significantly reduce the magnitude and variability of floor accelerations, brace forces, and connection forces, while maintaining comparable story drifts. Force-limiting connections primarily reduce the contribution of higher-mode responses, while the controlled rocking base mechanism modifies the first-mode response. Overall, the reduced dispersion in structural response improves the reliability of seismic design and enhances resilience by minimizing damage to both structural components and acceleration-sensitive nonstructural elements.

1. Introduction

The impact of natural hazards on society has created an urgent need of earthquake resilience and "better-than-code" buildings [1]. Various high-performance building systems, including systems with controlled rocking base mechanisms, have been developed to enhance post-earthquake functionality and reduce the structural damage [2–4]. Among these systems, self-centering concentrically braced frames (SC-CBFs) with controlled rocking base mechanism have emerged as a promising solution for steel buildings requiring enhanced seismic resilience.

SC-CBFs consist of three main components: 1) a stiff concentrically braced steel frame designed to remain essentially elastic, 2) vertical post-tensioning (PT) bars that provide overturning resistance and self-centering capability, and 3) ductile structural connections between the SC-CBFs and the foundation to control the rocking base mechanism. This design approach concentrates inelastic deformations at the rocking mechanism between the structural steel frame column elements and the foundation. The controlled controlled rocking base mechanism mitigates the first mode dynamic responses, reduces the residual drifts, and contributes to the faster post-earthquake recovery to a target functionality level.

Beginning in the early 2000s, major research initiatives supported by the U.S. National Science Foundation, primarily led by Lehigh University, Stanford University, and University of Illinois at Urbana-Champaign, advanced the development, experimental validation, and numerical modeling of SC-CBFs [5–13]. These studies confirmed the self-centering capabilities of the systems, evaluated component-level response, and provided data for calibrating computational models. Based on these findings, design methodologies and guidelines were proposed for SC-CBF systems. The research also identified key limitations, such as the effects of higher mode dynamic responses. The higher mode effects in SC-CBFs result in large member forces and floor accelerations. Therefore, heavy steel sections are required to maintain the elastic response of braces, beams, and columns of an SC-CBF [11].

Christopoulos and Zhong provided a review of the current state-of-the-art and state of research pertaining to the understanding, estimation, and mitigation of higher-mode effects on the seismic response of tall and slender reinforced concrete structures [14]. To control the higher-mode effects in rocking steel frames, Wiebe et al. proposed the use of

* Corresponding author.
E-mail addresses: gtsampras@ucsd.edu (G. Tsampras), rs0c@lehigh.edu (R. Sause).
URL: https://tsampras.ucsd.edu (G. Tsampras)

https://doi.org/10.1016/j.rcns.2025.12.004
Received 26 June 2025; Received in revised form 14 November 2025; Accepted 7 December 2025
Available online 18 December 2025
2772-7416/© 2025 The Author(s). Published by Elsevier B.V. on behalf of College of Civil Engineering, Tongji University. This is an open access article under the CC BY-NC-ND license (http://creativecommons.org/licenses/by-nc-nd/4.0/).

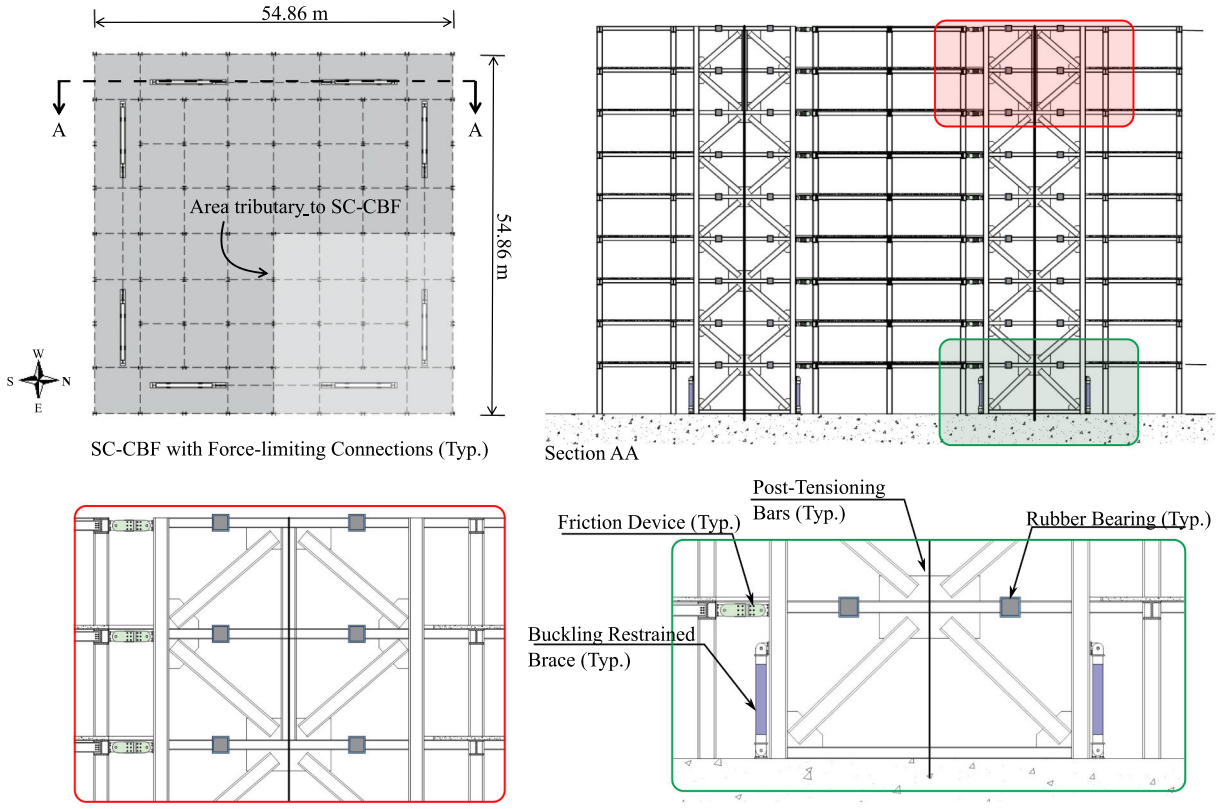


Fig. 1. Schematic structural details of nine-story SC-CBF building with force-limiting connections.

multiple rocking mechanisms above the controlled rocking base mechanism [15–17]. Practical force-limiting connections have been developed to reduce seismic-induced horizontal forces transferred between floors and the lateral force-resisting system (LFRS) and to mitigate higher-mode contributions [1,18–29]. A force-limiting connection in buildings with planar LFRS (e.g., reinforced concrete walls or rocking steel braced frames [19]) consists of a friction device or a buckling-restrained brace and low-damping rubber bearings. The force-limiting connections are designed to accommodate the seismic-induced three-dimensional kinematic requirements between floors and planar seismic force-resisting systems. The low-damping rubber bearings provide out-of-plane stability to planar seismic force-resisting systems and post-elastic stiffness to the force-limiting connections. The post-elastic stiffness in the force-limiting connections limits the seismic-induced displacement of the floors relative to the planar seismic force-resisting system. Overall, the use of force-limiting connections (1) limits the seismic-induced force and acceleration responses, (2) reduces the variability in the force and acceleration responses due to the ground motion variability, and (3) mitigates the effects of higher-mode responses on the dynamic response of buildings.

Building on prior research findings, the potential of force-limiting connections to mitigate higher-mode effects in SC-CBF systems needs to be studied. A detailed numerical study to evaluate the seismic performance of SC-CBF building models with force-limiting connections between the floor system and the LFRS is needed. To address this research gap, this manuscript presents results from numerical earthquake simulations of an SC-CBF building model with force-limiting connections.

2. Scope of study

This study numerically investigates the seismic response of a nine-story SC-CBF building that incorporates force-limiting connections between the floor system and the LFRS. The analysis focuses on the behavior of a building model under design basis earthquake (DBE) ground motions. A baseline SC-CBF model with rigid-elastic (RE) connection design is used for comparison.

The objective is to evaluate the influence of force-limiting connections on the seismic response, particularly in mitigating higher-mode effects. A force-based design method is employed to determine the limiting forces for the connections, and the effect of varying design force levels on performance is assessed. Emphasis is placed on quantifying reductions in floor accelerations, brace forces, and connection forces, as well as examining the variability of these responses across a suite of ground motions with differing characteristics. The potential for alternative design of the SC-CBF considering the beneficial effect of the force-limiting connections is beyond the scope of this paper and a topic for future research.

3. Building archetype

The building archetype considered in this study is a nine-story office building located in Los Angeles, California. The structural system consists of SC-CBFs placed in both orthogonal directions of the plan. The LFRS is located at the perimeter and connected to the gravity load resisting system (GLRS) through either RE or force-limiting connections. This configuration enables a direct assessment of the connection type on system performance. Fig. 1 shows the floor plan and structural details of the archetype building. The building is symmetric about the North-South and the East-West directions. The floor plan dimensions are 54.86 m x 54.86 m. The first story height is 4.57 m and the height of the rest of the stories is 3.96 m. Four SC-CBFs are used as seismic force resisting systems along each orthogonal floor plan direction. Close-up views of the base and the top stories of a SC-CBF are also shown.

The area tributary to one SC-CBF and the gravity system is shown in Fig. 1. The SC-CBF braces, SC-CBF columns, SC-CBF beams, SC-CBF base strut members were designed based on the design procedure and

Table 1
Summary of dead loads for SC-CBF building.

Source of Dead Load	Floors [kN/m^2]	Middle Floors [kN/m^2]	Roof [kN/m^2]
Floor/Roof Deck	0.14	0.14	0.14
Floor/Roof Slab	2.06	2.06	0.00
Roofing Material	0.00	0.00	0.48
Mechanical Weight	0.48	0.48	1.20
Ceiling Material	0.24	0.24	0.24
Floor Finish	0.10	0.10	0.00
Structural Steel	0.72	0.72	0.48
Steel Fireproofing	0.10	0.10	0.10
Building Envelope	0.37	0.34	0.25
Total	4.20	4.18	2.89

Table 2
Summary of live loads for SC-CBF building.

Source of Live Load	Floors [kN/m^2]	Roof [kN/m^2]
Office	2.39	0.00
Partitions (included in seismic mass)	0.72	0.00
Roof (unreduced)	0.00	0.96
Total	3.11	0.96

the design limit states presented in Chancellor et al. [12] and Roke [8]. This design procedure is performed in 25 steps and takes into account the higher mode effects in the computation of the design forces. The SC-CBF members were designed to remain elastic under DBE level ground motions. The effect of the force-limiting connections was not considered in the design of the SC-CBF. Tables 1 and 2 list the dead loads and live loads of the SC-CBF building. Table 3 lists the wide flange section member sizes in the SC-CBF. Low carbon structural steel with yield stress 345 MPa and modulus of elasticity 200 GPa was considered for the wide flange steel members. Ten post-tensioning bars were considered to be prestressed at initial pretension equal to 55 % of their yield stress 827 MPa. The design procedure results in a seismic response modification factor $R_{A,D-Drift} = 8$. The drifts predicted by the design procedure at decompression of the rocking base and at yielding of the PT steel are $\theta_D = 0.08\,\%$ and $\theta_{Y,n} = 1.6\,\%$, respectively. Tsampras [19] provides additional details on the design parameters of the nine-story SC-CBFs. Chancellor presented cyclic pushover curves that relate the overturning moment with the roof drift from experimental tests and numerical simulations of different building archetypes with SC-CBF [12] (Chapters 5 and 9).

The force-limiting connection used between each floor system and the SC-CBF consist of a friction device and low-damping rubber bearings (FD + RB). The force at which a force-limiting connection at floor level x transitions from the linear-elastic to the post-elastic response is the design limiting force (i.e., force-limiting connection design strength) F_{Lx}. The values of F_{Lx} are determined by the force-based design method proposed by the authors [19,30]. This method uses a modified version of design acceleration coefficients given by the Alternative Seismic Design Force for Floor Diaphragms per FEMA P-1050 [31]. The force-limiting connection design strength is computed as $F_{Lx} = (C_{Lx} w_{px})/(R_{DC} n_{Lx})$, where C_{Lx} is the design acceleration coefficient at level x, w_{px} is the seismic weight at level x, R_{DC} is the connection design force factor that accounts for the deformation capacity of the connection, and n_{Lx} is the number of force-limiting connections at level x. The parameters required to calculate C_{Lx} are the importance factor $I_e = 1.0$, the design spectral acceleration at short periods $S_{DS} = 1.0$, the design spectral acceleration at one second $S_{D1} = 0.6$, the mode shape factor $z_s = 1.0$, the seismic response acceleration coefficient $C_s = 0.0457$, higher mode seismic response acceleration coefficient $C_{s2} = 1.0$, the first mode contribution factor $\Gamma_{m1} = 1.4444$, the higher mode contribution factor (assuming one contribution factor for all the modes higher than the first mode) $\Gamma_{m2} = 0.7111$, the design acceleration coefficient at the base of the building $C_{Lo} = 0.4$, and the design acceleration coefficient at level n, $C_{Ln} = 0.7174$. R_{DC} equal to 1.5, 2.0, 2.5, 3.0, 5.0, 6.0, 7.0, and 8.0 was considered. Fig. 2 shows the eight sets of F_{Lx} for given R_{DC}. Smaller R_{DC} results in larger force-limiting connection design strength F_{Lx}. It is noted that the 8th floor F_{Lx} (i.e., F_{L8}) is the largest over the height of the building, because the seismic mass at the roof (i.e., 9th floor) is 59 % of the seismic mass at the 8th floor. If the seismic mass was uniform over the height of the building, F_{L9} would have the largest value compared to the rest of the floors. The seismic responses of the building model with force-limiting connections are compared with the seismic responses of the nine-story SC-CBF building model with RE connections to assess the effectiveness of the force-limiting connections to mitigate the higher-mode responses.

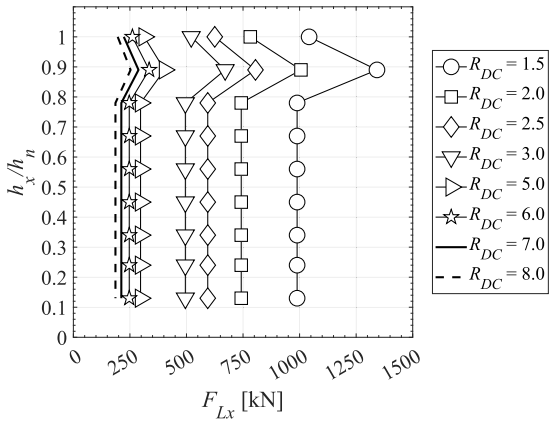


Fig. 2. Summary of F_{Lx} for nine-story SC-CBF building structure with various R_{DC} values.

4. Numerical model

Due to symmetry, one quarter of the building was studied using numerical earthquake simulations. OpenSees [32] was used to develop a two-dimensional numerical model. Fig. 3 shows the numerical model of the SC-CBF structure with force-limiting connections or RE connections. The SC-CBF design procedure ensures elastic response of the SC-CBF braces, SC-CBF columns, SC-CBF beams, SC-CBF base strut, and SC-CBF distribution struts. Elastic beam-column elements were used to model the SC-CBF beams, SC-CBF columns, SC-CBF braces, SC-CBF distribution strut, and SC-CBF base strut. Fig. 3 shows the details of the model at the foundation level. The modeling approach was adapted from Chancellor [11]. More specifically, the spring element E400 simulates the contact stiffness at the interface of the base plate of the SC-CBF column and the foundation. The foundation is not simulated explicitly. The foundation dimensions will be related to the number of stories and the expected reaction forces. Thus, the contact stiffness attempts to approximate the stiffness of the foundation as twice the axial stiffness of the column. The element E396 is a force-based beam-column element that represents the anchorage block of the PT bars. It has a very high stiffness (effectively rigid) and it is used to simulate the application of the initial displacement that results in the post-tension of the bars. PT yielding and slack was simulated. PT fracture was not simulated. PT yielding was simulated through the elasto-plastic material constitutive law assigned to the element E395 (ElasticPP). PT slack was simulated through the zero-length element E397 which has negligible tensile capacity and high elastic compressive stiffness. The distribution struts increase the stiffness of the post-tensioning bar load path and transfer the concentrated post-tensioning bar forces to the SC-CBF braces in the upper stories.

A pin-base lean-on column is used to model the GLRS. The lean-on column simulates the total stiffness of gravity columns within their

Table 3
Wide flange steel sections member sizes of SC-CBF.

Story/Floor	SC-CBF Columns	SC-CBF Braces	SC-CBF Beams	SC-CBF Distribution Strut	SC-CBF Base Strut
9	W14x176	W14x145	W12x96	W14x132	None
8	W14x176	W14x132	W12x96	W14x132	None
7	W14x176	W14x176	W12x96	None	None
6	W14x311	W14x132	W12x96	None	None
5	W14x311	W14x132	W12x96	None	None
4	W14x398	W14x132	W12x96	None	None
3	W14x398	W14x145	W12x96	None	None
2	W14x455	W14x211	W12x96	None	None
1	W14x455	W14x257	W12x96	None	W14x211

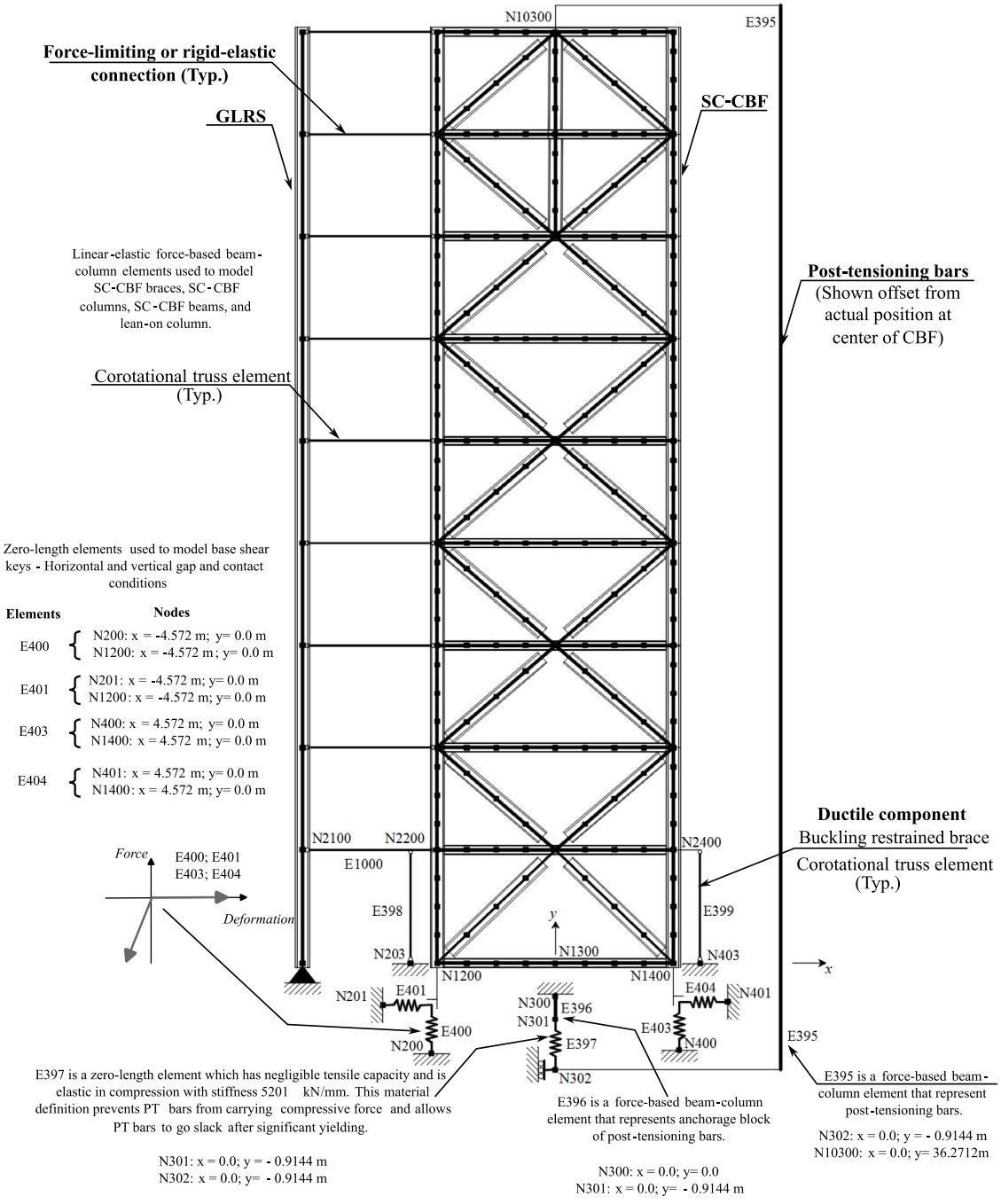


Fig. 3. Numerical model of nine-story SC-CBF building structure.

Table 4
Modal properties of SC-CBF building structure.

Mode [-]	T_n [seconds]	Γ_n [-]	M_n^* [MN/g]	M_n^*/M_{total} [-]
1	1.09	1.49	21.91	0.6920
2	0.30	-0.70	6.09	0.1923
3	0.17	0.37	1.77	0.0560
4	0.14	-0.27	0.68	0.0215

tributary area, assuming pinned beam-column connections within the gravity framing. The gravity loads are applied to the lean-on column. The flexibility of the floor diaphragm was not included in the model. Geometric nonlinearities are included in the numerical model. Rayleigh damping consisting of mass proportional damping and current stiffness proportional damping applied only to the SC-CBF beams, SC-CBF braces, SC-CBF columns, and the lean-on column is used to model the inherent damping of the SC-CBF building. The damping in the first and third modes was specified as 2.6 % and 6.1 %, respectively. These values of modal damping for the first and third mode match the modal damping used previously in laboratory testing of an SC-CBF [8]. An elastic-plastic force-deformation response with kinematic hardening is used to model the force-deformation response of the force-limiting connections. The elastic and post-elastic stiffness of the force-limiting connection models is equal to 1730 kN/mm and 8.65 kN/mm [24], respectively, for every force-limiting connection model in this study.

Table 4 lists the period, the modal participation factor, the modal effective mass, and the modal effective mass normalized by the total seismic mass for the first four modes of the building model.

5. Ground motions

The Far Field (FF) set of twenty-two pairs of ground motion records (forty-four in total) proposed by FEMA-P695 [33] is used to define the set of ground motion records considered in this study. These ground motions were recorded during events with magnitude $M \in [6.5\ 7.6]$ at sites at least 10 km from the fault. The set includes ground motions dominated by shallow crustal earthquakes (occur within 30 km of the surface) with either strike-slip or reverse (thrust) sources, representative of areas in Western United States. Most of the ground motions in the set have been recorded on either soft rock (Site Class C) or stiff soil (Site Class D) sites. The lower limit of peak ground acceleration (PGA) and peak ground velocity (PGV) is 0.2 g and 15 cm/sec, respectively. This set of ground motions includes records of ground acceleration time histories available in the PEER NGA database [34]. Additional details are provided in Appendix A.7 and Appendix A.9 of FEMA-P695 [33].

A subset of ground motion records was determined after scaling the original records to match the ASCE/SEI 7 design pseudo-acceleration spectrum [35], computing the summation of the squared errors (SSE) between the spectral pseudo-acceleration of the scaled records and the design spectral pseudo-acceleration, and selecting the eighteen ground motion records that resulted in $SSE \leq \mu_{SSE}$, where μ_{SSE} is the mean value of SSE. Scaling was performed considering the spectral pseudo-accelerations within the period range $T \in [0.6, 2.0]$ seconds with a period increment $\Delta T = 0.01$ seconds resulting in $N_T = 141$ period samples, which is greater than the 50 period samples per order of magnitude in the period range recommended by Baker [36]. The ASCE/SEI 7 design spectrum parameters used for the design of the building archetype are $S_1 = 0.6$ g, $S_s = 1.5$ g, $F_a = 1.0$, $F_v = 1.5$, $T_{long} = 8.0$ seconds, Site Class D, and $I_e = 1.0$ [35]. The scale factors and SSE were computed according to Eqs. (1) and (2), respectively:

$$SF_i = \frac{\frac{1}{N_T}\sum_{j=1}^{N_T} SA_d(T_j)}{\frac{1}{N_T}\sum_{j=1}^{N_T} SA_i(T_j)} = \frac{\sum_{j=1}^{N_T} SA_d(T_j)}{\sum_{j=1}^{N_T} SA_i(T_j)} \quad (1)$$

$$SSE = \sum_{j=1}^{N_T} \left[\ln SA_i(T_j) - \ln SA_d(T_j)\right]^2 \quad (2)$$

where SF_i is the scale factor for the i^{th} ground motion, $SA_i(T_j)$ is the spectral pseudo-acceleration of the i^{th} ground motion at a period T_j ($j = 1, 2, 3, \ldots N_T$), $SA_d(T_j)$ is the target design spectral pseudo-acceleration at a period T_j. $\ln SA_i(T_j)$ and $\ln SA_d(T_j)$ are the natural logarithm of the spectral pseudo-accelerations. The scaled ground motion, median, and design pseudo-acceleration, pseudo-velocity and displacement spectra are plotted in Fig. 9 assuming 5 % damping ratio.

Table 5 lists the unique IDs, the name of the event, the magnitude, the year, the record name, the component name, and the scale factor for each ground motion record used in this study. It is shown that the range of scale factors was between 0.71 and 2.77, with three records having a factor larger than 2.0. Research suggests that scale factors up to 4 may be acceptable [37–39]. However, scaling of ground motion records for use in earthquake numerical simulations is not unanimously accepted [40,41]. For the purpose of comparing the seismic response of SC-CBF building model with and without force-limiting connections, it is assumed that the scale factors used for the numerical earthquake simulations presented in the next section are acceptable.

6. Numerical earthquake simulations

6.1. Variations of SC-CBF model

Nine floor-to-LFRS connection design cases are considered to develop nine variations of the SC-CBF model. The first connection design case assumes an effectively rigid linear elastic floor-to-LFRS connection. This is the baseline connection design case and it is termed RE connection design. Eight additional connection design cases are considered assuming force limiting connections designed with the F_{Lx} shown in Fig. 2. Smaller R_{DC} indicates larger force-limiting connection design strength F_{Lx}. The response of the SC-CBF model with RE connection design is compared with the response of the SC-CBF models with various force-limiting connection design strengths F_{Lx}. Each SC-CBF model is subjected to the eighteen scaled earthquake ground motions listed in Table 5.

6.2. Results

Fig. 4 shows the structural seismic responses computed for the SC-CBF model with different connection design cases. The figure shows the floor total acceleration, the connection force, the left brace axial force, the right brace axial force, the GLRS story shear, the connection deformation, the LFRS story drift ratio, and the GLRS story drift ratio. The horizontal axis shows either the floor level or the story level. Each marker on the figure represents the peak (i.e., maximum absolute) value from the time-history response and the maximum value of the responses. The color of the markers indicates the different connection design cases. The eighteen markers at each floor level or story level for each connection design case indicate results from the eighteen ground motions. The mean value of the peak responses from the eighteen ground motions (termed the mean peak values) is shown with a white marker. Table 6 lists the mean μ and coefficient of variation σ/μ of the responses for each connection design case plotted in Fig. 4. More specifically, μ is the maximum mean peak value over the height of the building model and σ is the standard deviation associated with μ. The statistics are plotted in Fig. 5 as a function of the connection design case.

6.2.1. Floor total accelerations

The mean peak floor total accelerations in the SC-CBF model with RE connection design are significantly larger compared to the mean peak floor total accelerations in the SC-CBF model with force-limiting connections at every floor except for the seventh floor. The seventh floor is

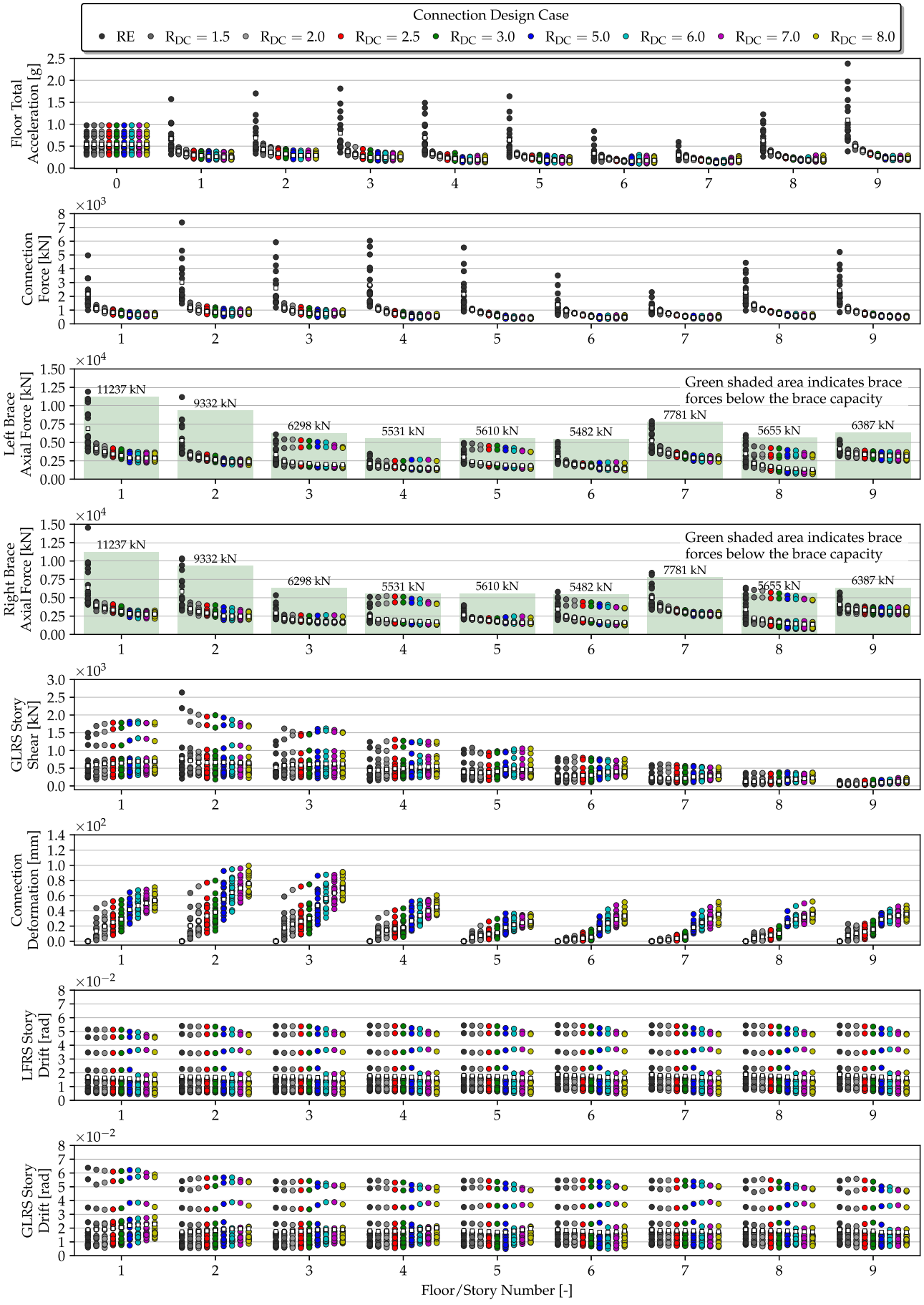


Fig. 4. Seismic responses in nine-story SC-CBF building model with different connection designs.

Table 5
Earthquake event data with ground motion parameters.

ID [-]	Event [-]	M [-]	Year [-]	Distance [km]	Soil Type [-]	Component [-]	*PGA [g]	*PGV [cm/sec]	**SF [-]
EQ1	Friuli Italy	6.5	1976	15.0	C	TMZ000	0.35	22	2.77
EQ2	Duzce Turkey	7.1	1999	12.0	D	BOL000	0.73	56	0.99
EQ3	Superstition Hills	6.5	1978	11.2	D	B-POE270	0.45	36	1.87
EQ4	Superstition Hills	6.5	1978	11.2	D	B-POE360	0.30	33	1.97
EQ5	Chi-Chi Taiwan	7.6	1999	10.0	D	E - W	0.35	71	1.33
EQ6	Chi-Chi Taiwan	7.6	1999	10.0	D	N - S	0.44	115	0.84
EQ7	Landers	7.3	1992	19.7	D	CLW-LN	0.28	26	2.54
EQ8	Imperial Valley	6.5	1979	22.0	D	H-DLT262	0.24	26	1.90
EQ9	Imperial Valley	6.5	1979	22.0	D	H-DLT352	0.35	33	1.28
EQ10	Imperial Valley	6.5	1979	12.5	D	H-E11230	0.38	42	2.06
EQ11	Northridge	6.7	1994	9.4	D	MUL279	0.52	63	0.71
EQ12	Superstition Hills	6.5	1978	18.2	D	ICC000	0.36	46	1.42
EQ13	Loma Prieta	6.9	1989	12.2	D	G03090	0.37	45	1.40
EQ14	Kocaeli Turkey	7.5	1999	13.6	D	DZC180	0.31	59	1.53
EQ15	Kocaeli Turkey	7.5	1999	13.6	D	DZC270	0.36	46	0.93
EQ16	Cape Mendocino	7.0	1992	7.9	D	RIO270	0.39	44	1.27
EQ17	Kobe Japan	6.9	1995	19.1	D	SHI090	0.21	28	1.66
EQ18	Landers	7.3	1992	23.6	D	YER270	0.24	51	1.24

*From original earthquake ground motion records
**SF: Scale Factor to match design spectral accelerations over period range T∈[0.6, 2.0] seconds

Table 6
Statistics of seismic responses.

Connection Design Case	Floor		Connection				LFRS						GLRS			
	Total Acceleration		Force		Deformation		Left Brace Force		Right Brace Force		Drift		Shear		Drift	
	μ	$\frac{\sigma}{\mu}$	μ	$\frac{\sigma}{\mu}$	μ	$\frac{\sigma}{\mu}$	μ	$\frac{\sigma}{\mu}$	μ	$\frac{\sigma}{\mu}$	μ	$\frac{\sigma}{\mu}$	μ	$\frac{\sigma}{\mu}$	μ	$\frac{\sigma}{\mu}$
[−]	[g]	[−]	[kN]	[−]	[mm]	[−]	[kN]	[−]	[kN]	[−]	[rad]	[−]	[kN]	[−]	[rad]	[−]
RE	1.09	0.49	3010	0.52	0.00	0.52	6880	0.40	6389	0.44	0.019	0.73	767	0.84	0.019	0.73
R_{DC} = 1.5	0.50	0.06	1351	0.07	20.26	0.80	4190	0.09	3977	0.09	0.018	0.75	713	0.71	0.019	0.83
R_{DC} = 2.0	0.39	0.05	1056	0.03	26.80	0.63	3735	0.09	3578	0.08	0.018	0.77	664	0.73	0.020	0.82
R_{DC} = 2.5	0.33	0.20	887	0.17	33.30	0.50	3422	0.10	3321	0.10	0.018	0.79	658	0.74	0.020	0.78
R_{DC} = 3.0	0.32	0.21	830	0.18	38.11	0.44	3297	0.11	3261	0.11	0.018	0.79	663	0.72	0.020	0.76
R_{DC} = 5.0	0.29	0.21	780	0.19	55.30	0.31	3175	0.12	3166	0.11	0.017	0.83	683	0.68	0.022	0.70
R_{DC} = 6.0	0.29	0.20	808	0.16	64.12	0.24	3170	0.13	3149	0.11	0.017	0.85	693	0.67	0.022	0.68
R_{DC} = 7.0	0.29	0.18	827	0.14	70.00	0.19	3133	0.12	3145	0.11	0.016	0.85	694	0.66	0.023	0.64
R_{DC} = 8.0	0.29	0.18	852	0.13	75.87	0.16	3116	0.12	3136	0.11	0.016	0.84	693	0.64	0.023	0.61

located close to the node of the second mode shape where the contribution of the second mode to the total dynamic response of the building is expected to be low. The SC-CBF model with RE connection design subjected to EQ7 results to the overall maximum peak (i.e., over all floors and ground motions) floor total acceleration. The dispersion of the peak floor total accelerations for the SC-CBF model with RE connection design is significantly larger than the dispersion of the peak floor total accelerations for the SC-CBF model with force-limiting connections. μ reduces as the R_{DC} increases from 1.5 to 5.0 and it is constant for R_{DC} between 5.0 and 8.0.

6.2.2. Connection forces

The force-limiting connections transfer the seismic-induced inertia forces from the floors to the LFRS. The inertia forces are proportional to the floor total acceleration. As a result, the observations made in the previous section about the floor total acceleration apply to the connection forces. The mean peak connection forces in the SC-CBF model with RE connection design are significantly larger compared to the mean peak connection forces for the SC-CBF model with force-limiting connections at every floor except the seventh floor. The SC-CBF model with RE connection design subjected to EQ7 results to the overall maximum peak connection force. The dispersion of the peak connection forces for the SC-CBF model with RE connection design is significantly larger than the dispersion of the peak connection forces for the SC-CBF model with force-limiting connections. μ reduces as the R_{DC} values increase from 1.5 to 5.0 and it is constant for R_{DC} values from 5.0 to 8.0. The mean peak values of connection forces shown in Fig. 4 are similar to the F_{Lx} for R_{DC} =1.5 shown in Fig. 2. The differences between F_{Lx} and the mean peak values of the connection forces are attributed primarily to the post-elastic deformation demand.

6.2.3. Connection deformations

The maximum mean peak connection deformations in the SC-CBF building model with force-limiting connections are reasonable and smaller than 100 mm; the upper limit for the design level deformations defined for the original development of the force-limiting connections [19,22]. This is possible because of the effectiveness of F_{Lx} in the determination of the forces required to design the force-limiting connections [30]. The maximum peak connection deformation is located at the second floor for all connection design cases. As listed in Table 6, μ for R_{DC} =1.5 and 2.0 is limited to 20 mm and 27 mm, respectively.

6.2.4. Story drifts

The magnitude and variability of the mean peak LFRS and GLRS story drifts in the SC-CBF model with RE connection design are similar to those of the LFRS and GLRS story drifts of the SC-CBF model with force-limiting connections, respectively. EQ5, EQ6 and EQ14 lead to large LFRS story drifts and GLRS story drifts in all connection design cases. The SC-CBF model with RE connection design subjected to EQ6 results to the overall maximum peak LFRS and GLRS story drifts.

6.2.5. Brace axial forces

The magnitude and variability of the mean peak brace axial forces in the SC-CBF model with RE connection design are larger compared to the

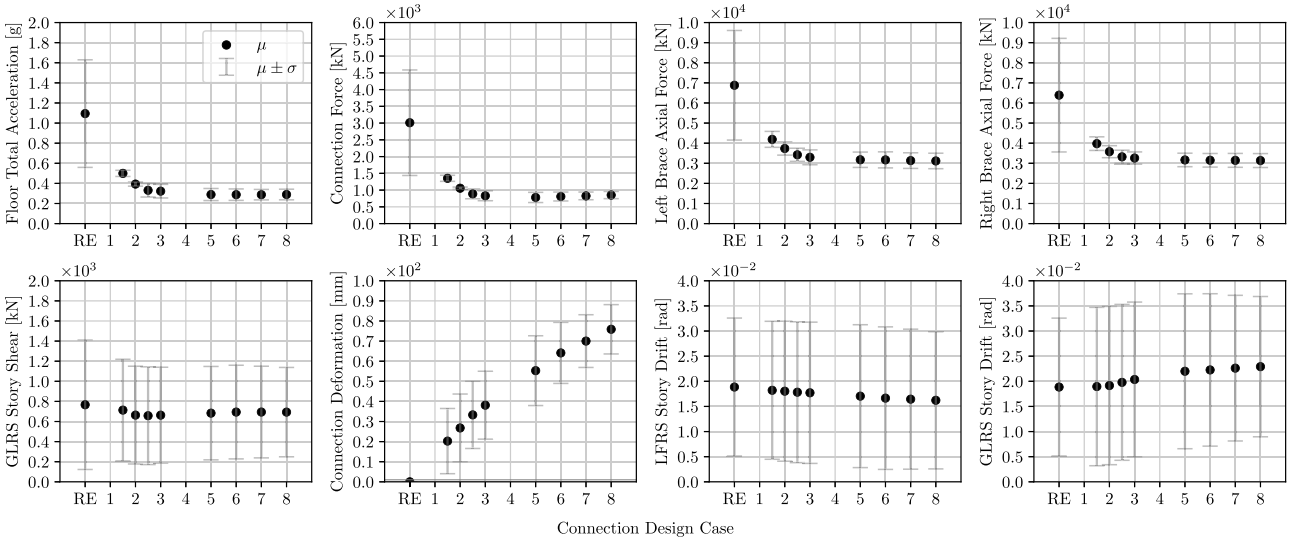


Fig. 5. Statistics of seismic responses in nine-story SC-CBF building model with respect to connection design case.

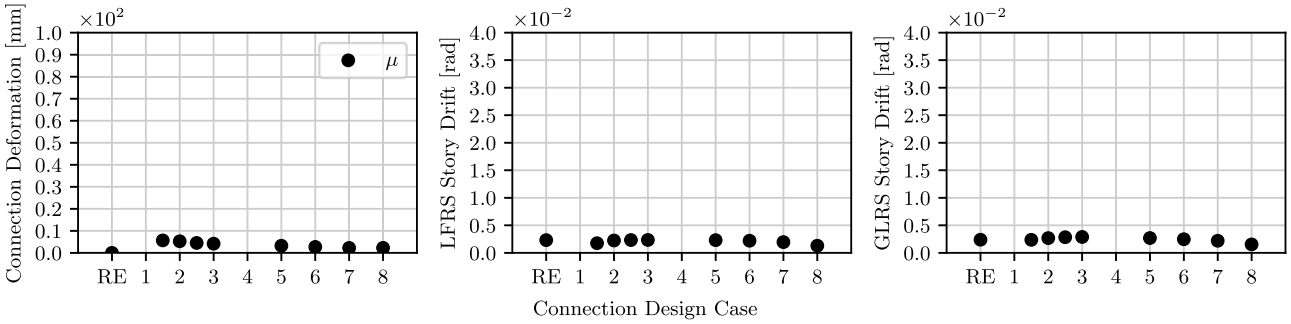


Fig. 6. Mean residual connection deformation and story drifts in the nine-story SC-CBF building model with respect to connection design case.

mean peak brace axial forces in the SC-CBF model with force-limiting connections. The SC-CBF model with RE connection design subjected to EQ7 results in the overall maximum peak brace force. μ reduces as the R_{DC} values increase from 1.5 to 5.0 and it is constant for R_{DC} values from 5.0 to 8.0. All connection design cases indicate that the maximum mean peak values occur at the first story. The mean peak values progressively reduce from the first to the fifth story. From the fifth to the seventh story, they increase again to reach the second local maximum (the first being the overall maximum at the first story).

The variability is associated with the large brace axial forces from the two ground motions, which result in large drift demands. Thus, they are driven by the characteristics of the ground motions. The reason they appear with one story offset is that the SC-CBF uses a two story X-brace configuration, and at the gusset at the beam midspan, the right brace above transfers the axial load to the left brace in the story below. This is why the axial force magnitude for these large force cases is similar in the stories above and below. In the case of the 8th story, the distribution strut helps with the redistribution of the forces. The 8th story is expected to experience large brace forces due to the higher mode effects that are significant at the top 20 % height of the structure compared to the rest of the structure.

The overall maximum peak brace forces are similar or lower than the brace design capacity forces, which are controlled by axial compression. The brace capacity forces in story 9, 8, 7, 6, 5, 4, 3, 2, and 1 are 6387 kN, 5655 kN, 7781 kN, 5482 kN, 5610 kN, 5531 kN, 6298 kN, 9332 kN, 11237 kN, respectively. One of the ground motions that resulted in large drift demand, also resulted in brace peak forces approximately equal to or larger than the corresponding capacity of the brace. Considering the overall results, the linear elastic brace models used in this comparative study are deemed appropriate for this study.

The reduced brace forces when force-limiting connections are used indicate that the SC-CBF could be designed with lighter steel sections. The SC-CBF with force-limiting connections was not re-designed in this study to ensure the direct comparison of the responses with the SC-CBF with RE connections. The holistic design of systems with force-limiting connections is beyond the scope of this paper. A resilience-based design method for the design of buildings with floor-to-LFRS force-limiting connections and rocking base mechanism is currently under development [42].

6.2.6. *GLRS story shears*

The use of force-limiting connections instead of RE connections practically does not affect the magnitude and variability of the GLRS story shears in the SC-CBF model. The SC-CBF model with RE connection design subjected to EQ6 has the overall maximum peak GLRS story shear.

6.2.7. *Residual responses*

Fig. 6 shows the maximum (over the height of the building model) mean residual connection deformation and story drifts with respect to R_{DC}. The maximum mean residual connection deformation for all connection design cases with force-limiting connections ranges approximately between 2 mm and 6 mm while the maximum mean residual story drifts range approximately between 0.2 % and 0.3 %. The residual drifts are possible because of the nonlinear inelastic stress-strain response of the PT bars. At drifts approximately equal to 1.6 % initiation of yielding in the PT bars is expected. The nonlinear inelastic response

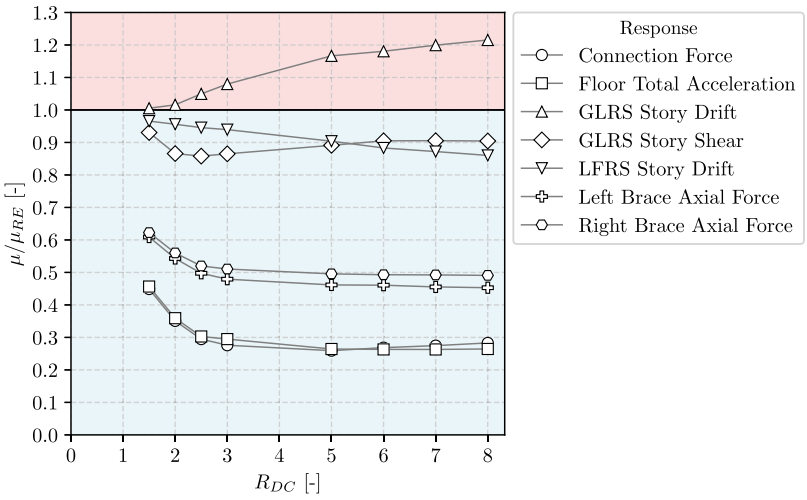


Fig. 7. Effect of R_{DC} on μ normalized with respect to μ values for the SC-CBF model with RE connection design.

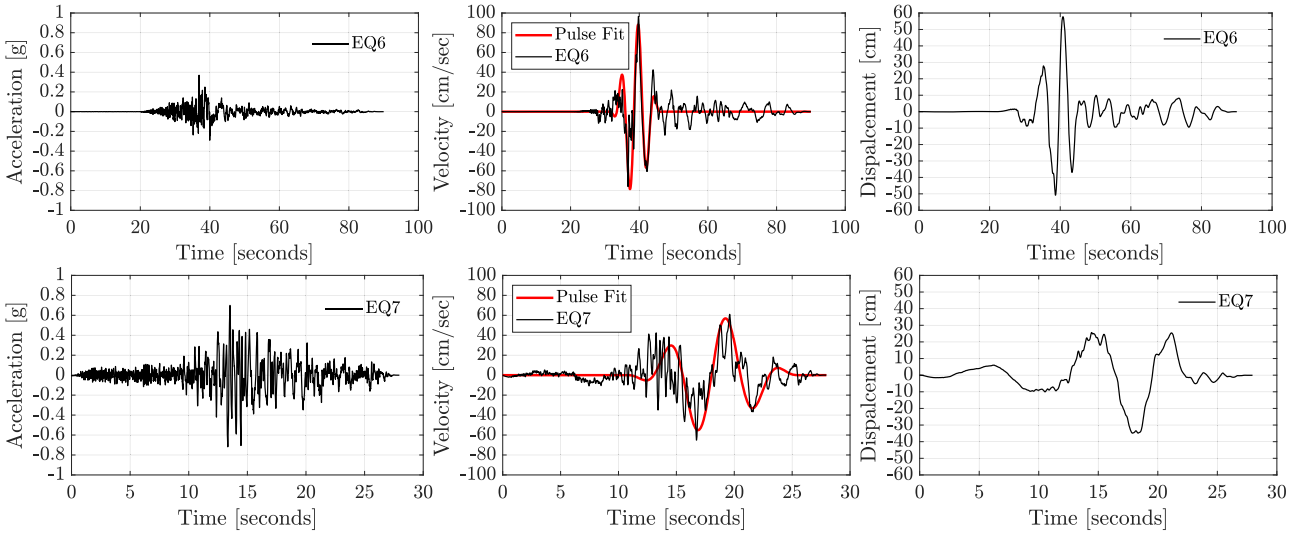


Fig. 8. EQ6 and EQ7 scaled earthquake ground motion record time histories.

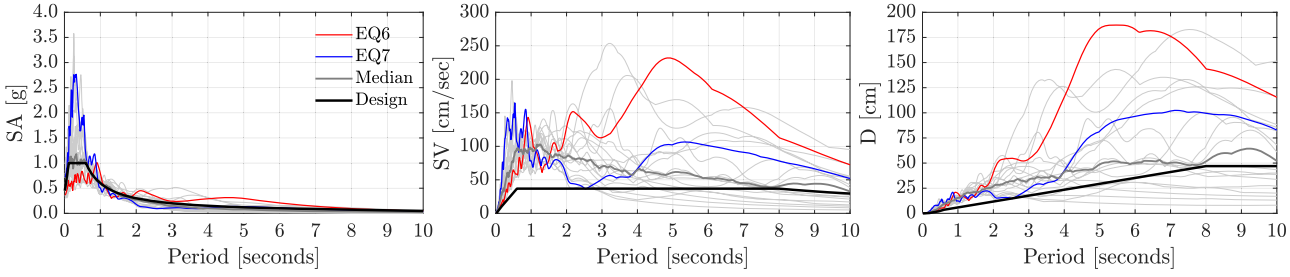


Fig. 9. Ground motion pseudo-acceleration, pseudo-velocity and displacement spectra for EQ6 and EQ7 assuming 5 % damping ratio.

of the PT bars and the buckling restrained braces at the rocking base of the SC-CBF result in the residual drift.

6.2.8. *Normalized responses with respect to R_{DC}*

Fig. 7 shows μ for all the seismic responses, except for the connection deformation, normalized by μ for the SC-CBF model with RE connection design, termed μ/μ_{RE}, with respect to R_{DC}. The plot concisely summarizes the significant effect of force-limiting connections on the floor total accelerations, connection forces, and brace axial forces. Analysis cases with R_{DC} =1.5, 2.0, and 2.5 result in small μ/μ_{RE} for the floor total accelerations, connection forces, and brace axial forces while μ/μ_{RE} for the GLRS story shears ranges between 0.85 to 0.95 and without significantly affecting the LFRS and GLRS story drift. As a result, the authors recommend the use of R_{DC} between 1.5 and 2.5. These results align with the results observed for cast-in-place reinforced concrete wall systems with force-limiting connections [30]. More specifically, in the case of cast-in-place reinforced concrete wall systems with force-limiting connections, it was observed that values of R_{DC} close to 1.5 for the twelve- and eight-story buildings and 1.0 for the four-story buildings result in acceptable seismic responses.

The authors do not recommend the use of R_{DC} values greater than 2.5 due to the potential for large GLRS drift demand without further

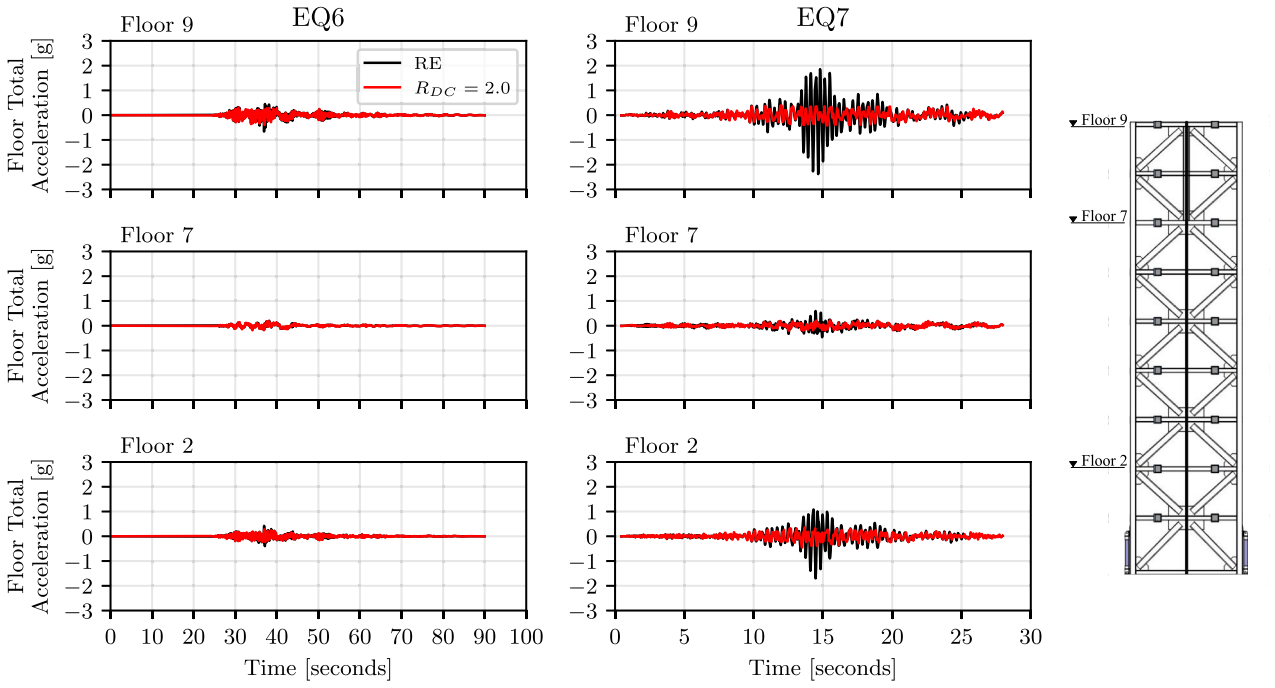


Fig. 10. Floor total acceleration for RE and R_{DC} = 2.0 connection design cases due to EQ6 and EQ7.

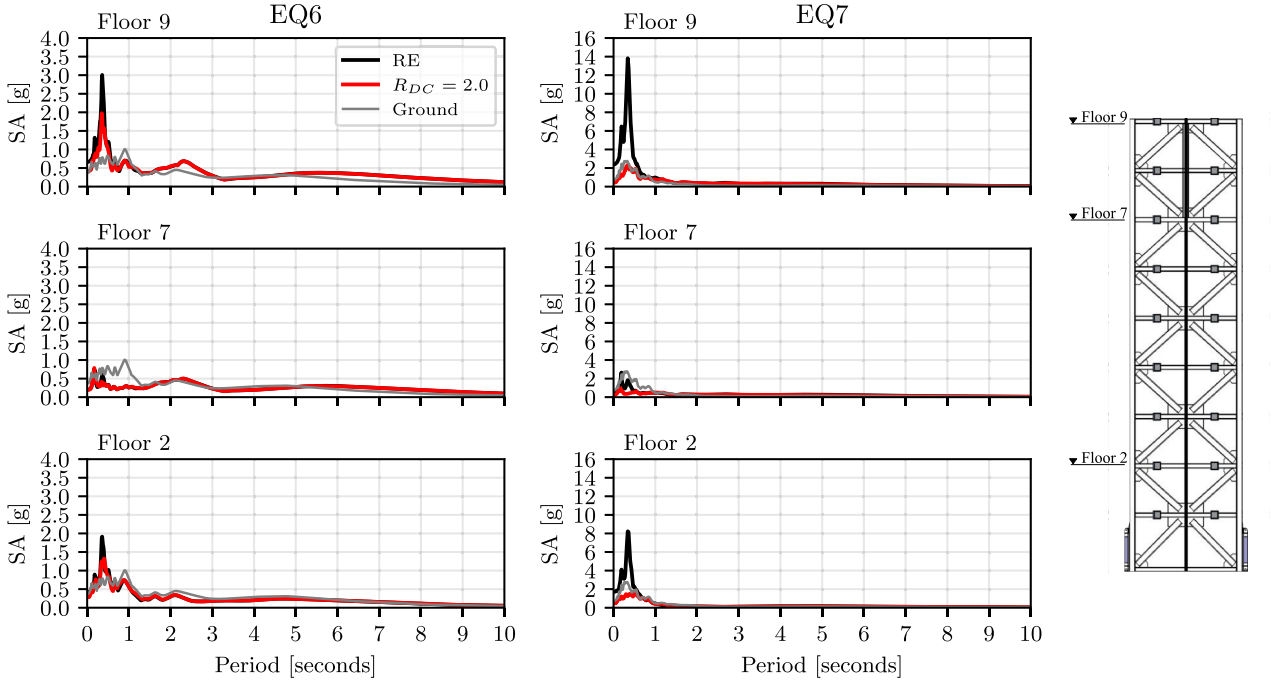


Fig. 11. Floor pseudo-acceleration spectra for RE and R_{DC} = 2.0 connection design cases due to EQ6 and EQ7.

reduction in the force and acceleration responses compared to R_{DC} between 1.5 and 2.5. R_{DC} values lower than 1.5 could be used assuming that (1) limited ductility is required from the force-limiting connections at the design level earthquake, (2) the majority of the ductility demand is expected to be concentrated at the rocking base mechanism, (3) smaller reduction in force and acceleration responses compared to the reductions expected with R_{DC} between 1.5 and 2.5 is acceptable.

6.2.9. Response to EQ6 and EQ7

This section focuses on connection design cases RE and R_{DC} = 2.0 considering the two scaled ground motion records EQ6 and EQ7. EQ6 led to large drift demands and EQ7 led to large force and acceleration demands. The goal is to assess the contribution of the first mode and higher mode responses to the total dynamic response of the SC-CBF model. The reasons for the reductions in the force- and acceleration-related structural responses and the large drift are discussed.

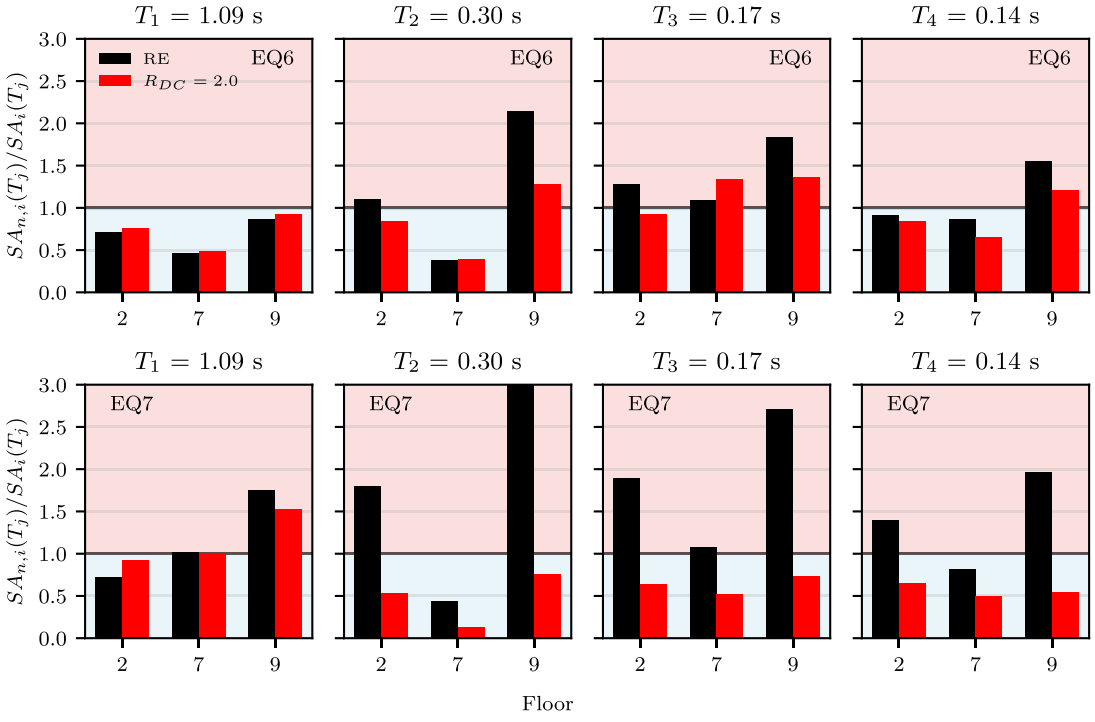


Fig. 12. Normalized floor pseudo-acceleration spectral values for RE and $R_{DC} = 2.0$ connection design cases due to EQ6 and EQ7.

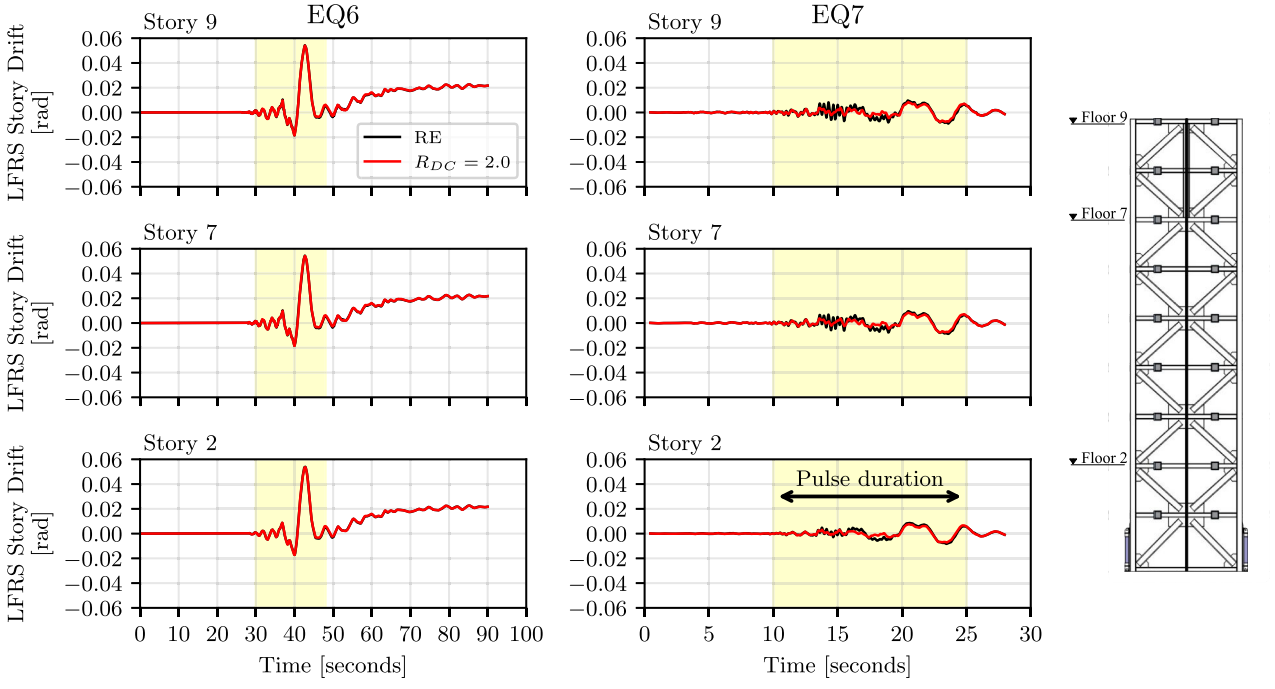


Fig. 13. LFRS story drift for RE and $R_{DC} = 2.0$ connection design cases due to EQ6 and EQ7.

Fig. 8 shows the acceleration, velocity, and displacement time histories of the scaled ground motion records EQ6 and EQ7. The scale factors used for EQ6 and EQ7 were 0.84 and 2.54 (see Table 5), respectively. EQ7 has a larger peak ground acceleration compared to EQ6. The ground motion records have a similar duration of strong motion excitation (approximately 25 seconds). As discussed previously, the ground motion records are part of the FEMA P695 far-field ground motion set. However, pulses are observed in the EQ6 and EQ7 velocity time histories. The mathematical representation of near-fault ground motions proposed by Mavroeidis and Papgeorgiou [43] described in Eq. (3) was used to fit velocity pulses on the EQ6 and EQ7 velocity time histories.

$$\dot{u}(t) = A\frac{1}{2}\left[1 + \cos\left(\frac{2\pi f_P}{\gamma}(t - t_0)\right)\right]\cos\left[2\pi f_P(t - t_0) + \nu\right],$$

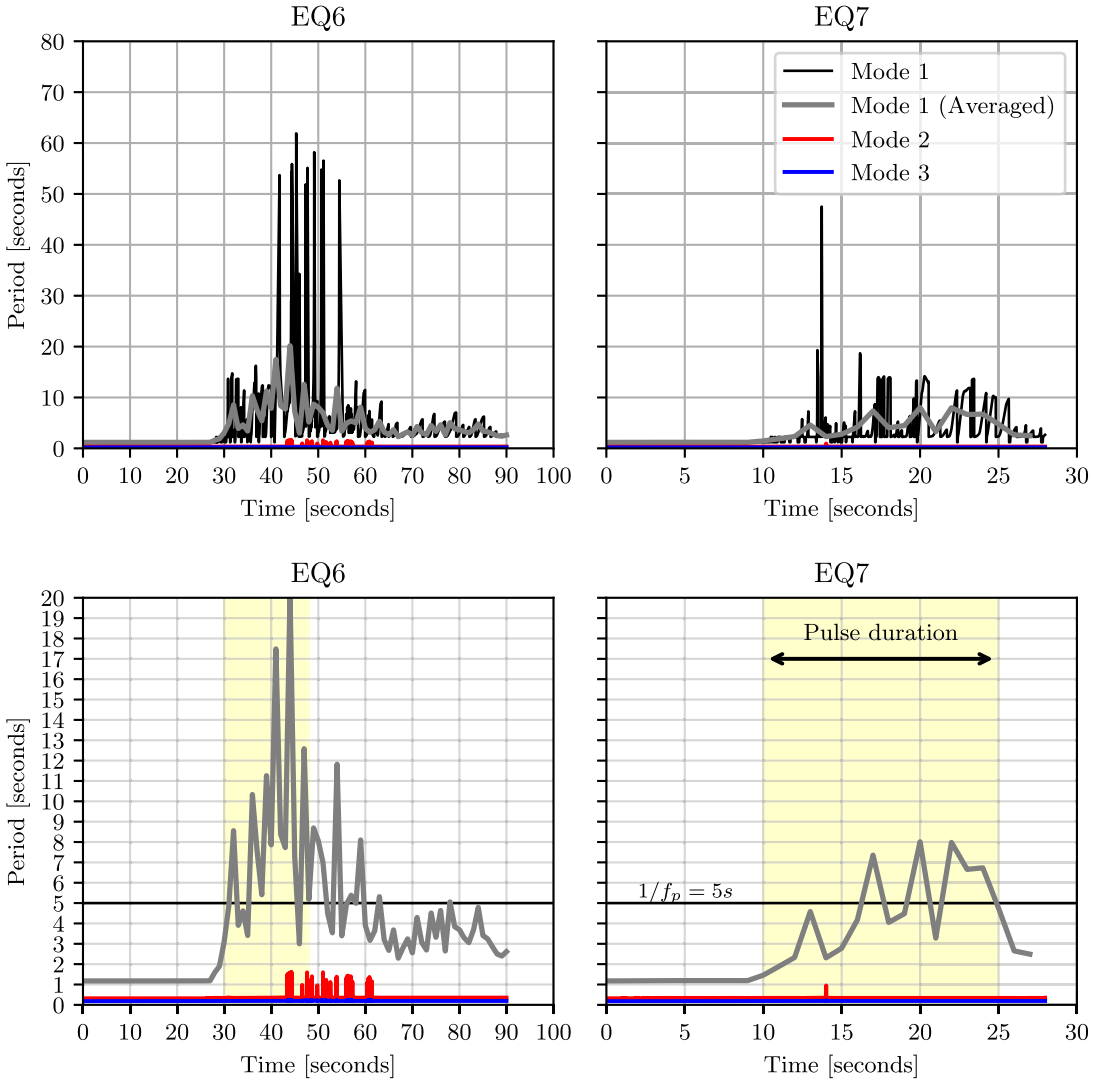


Fig. 14. Modal periods computed through eigenvalue analysis at each converged time step of the nonlinear earthquake simulations for RE connection design case due to EQ6 and EQ7.

$$\text{where} \quad t_0 - \frac{\gamma}{2f_P} \le t \le t_0 + \frac{\gamma}{2f_P} \quad \text{with } \gamma > 1 \tag{3}$$

where A controls the amplitude of the simulated pulse velocity time history, f_P is the frequency of the amplitude-modulated harmonic, ν is the phase of the amplitude-modulated harmonic, γ is a parameter that defines the oscillatory character of the signal, and t_0 specifies the epoch of the envelope's peak. $A = 90.0$ cm/sec and 60.0 cm/sec for EQ6 and EQ7, respectively. $\nu = -70.0°$ and $-70.5°$ for EQ6 and EQ7, respectively. $t_0 = 39.0$ seconds and 18.2 seconds for EQ6 and EQ7, respectively. $f_P = 1/5.0$ Hz and $\gamma = 3.0$ for EQ6 and EQ7.

The mathematically simulated velocity pulses with 5.0 seconds period ($f_p = 1/5.0$ Hz) fit reasonably well the velocity time histories. The velocity magnitude in EQ6 is larger compared to EQ7. Considering the amplitude of the velocity pulse in EQ6 is approximately 90 cm/seconds, a relatively high energy near-fault type excitation can be assumed (energy is proportional to the square of the velocity).

Fig. 9 shows the spectral pseudo-acceleration, SA, the spectral pseudo-velocity, SV, and the spectral displacement, D, of the eighteen scaled ground motion records with light gray. The red and blue lines highlight the spectral quantities for EQ6 and EQ7. The design spectra are shown with black lines. EQ7 has high SA compared to the design spectral acceleration close to the second mode period ($T_2 = 0.3$ seconds), while EQ6 has relatively low SA values close to the second mode period. EQ7 has large SV and D values close to a period of 5.0 seconds. This observation is expected considering the 5.0 seconds period large amplitude velocity pulse identified in EQ7.

Based on observations from the two ground motions, EQ6 is expected to predominantly excite the first-mode nonlinear dynamic response of the SC-CBF model, while EQ7 is expected to primarily excite higher-mode nonlinear responses. The following discussion focuses on the acceleration responses at the second, seventh, and ninth floors for the RE and $R_{DC} = 2.0$ connection design cases under both EQ6 and EQ7.

These specific floors are selected for the following reasons: 1) The seventh floor is located near the nodal point of the second mode shape. 2) The second and ninth floors are situated at elevations where the combined contributions of the second, third, and fourth modes are expected to significantly influence the floor total acceleration. 3) Relatively high mean peak floor total accelerations were observed at the second and ninth floors (see Fig. 4). 4) Conversely, relatively low mean peak floor total accelerations were observed at the seventh floor.

Fig. 10 presents the total acceleration time histories at the ninth, seventh, and second floors for the RE and $R_{DC} = 2.0$ connection design cases under ground motions EQ6 and EQ7. For the RE case, EQ7

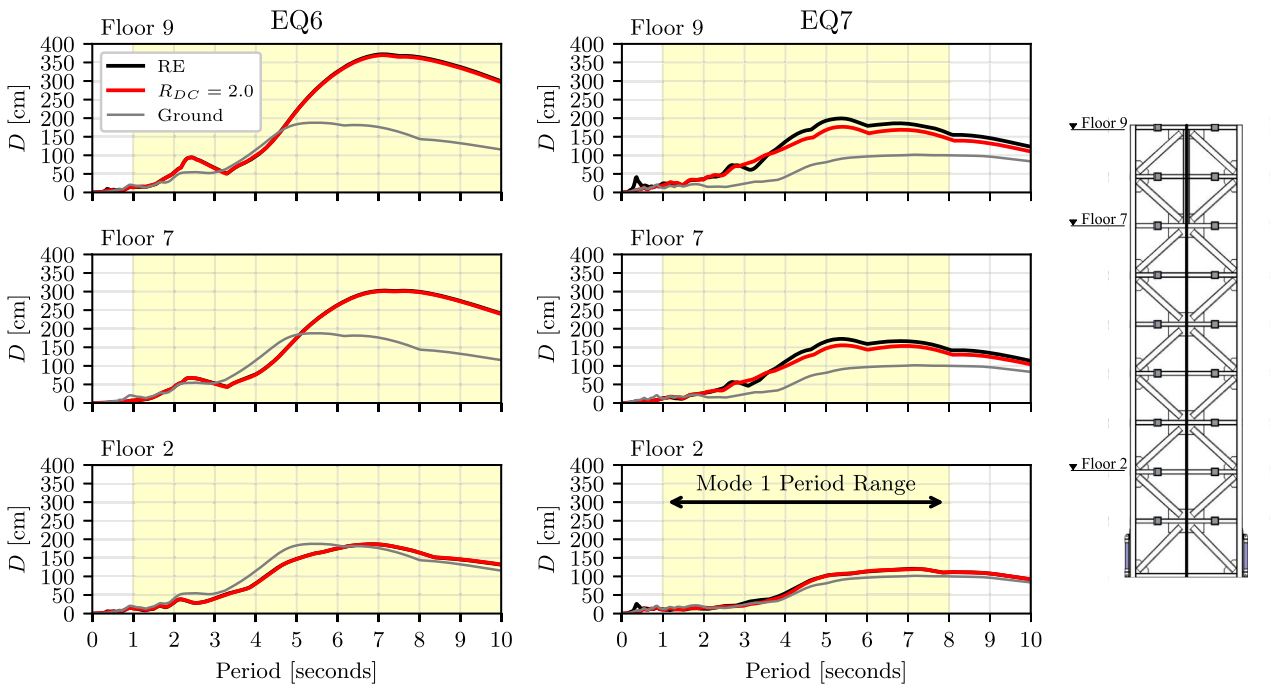


Fig. 15. Floor displacement spectra for RE and R_{DC} = 2.0 connection design cases due to EQ6 and EQ7.

produces relatively high total accelerations at both the ninth and second floors. These acceleration demands are notably reduced in the $R_{DC} = 2.0$ case. At the seventh floor, located near the node of the second mode, low total accelerations are observed in both connection design cases under EQ6 and EQ7.

Fig. 11 shows the floor pseudo-acceleration response spectra, SA, computed from the total acceleration time histories at the same floors and connection design cases. In the period range corresponding to the second mode, the RE case under EQ7 results in substantially larger SA values at the ninth and second floors compared to both the ground and the $R_{DC} = 2.0$ case.

Fig. 12 shows the floor pseudo-acceleration spectral values normalized by the ground spectral acceleration values, termed $SA_{n,i}(T_j)/SA_i(T_j)$, considering the ground motions EQ6 and EQ7, the connection design case RE and $R_{DC} = 2.0$, and the period of the first four modes of the SC-CBF model listed in Table 4. $SA_i(T_j)$ was defined previously and $SA_{n,i}(T_j)$ represents the spectral pseudo-acceleration computed using the floor total acceleration time history at floor n for ground motion i at period T_j. $SA_{n,i}(T_1)/SA_i(T_1)$ are similar in both connection design cases. The differences observed in higher mode periods are more significant in EQ7 compared to EQ6. Specifically, the use of force-limiting connections in connection design case $R_{DC} = 2.0$ results in significantly lower $SA_{n,i}(T_j)/SA_i(T_j)$ for EQ7 computed using the second and ninth floor total accelerations at second mode, third mode, and fourth mode periods compared to connection design case RE.

In conclusion, the use of force-limiting connections between the floors and the LFRS in the SC-CBF model results in control (i.e., reduction) of the higher mode acceleration responses. The limitation of the higher mode responses is responsible for the reduction in the mean peak values and the ground motion-to-ground motion variability in the force and acceleration sensitive structural responses observed in Fig. 4. The use of force-limiting connections does not significantly affect the first mode dominant dynamic responses (i.e., story drift). In the next paragraphs, the LFRS story drift time histories along with the displacement spectra are studied to evaluate the contribution of the first mode to the story drift of the SC-CBF building model.

Fig. 13 shows the ninth story, seventh story, and second story LFRS drift time histories for RE and $R_{DC} = 2.0$ connection design cases due to EQ6 and EQ7. Almost identical LFRS story drift time histories are observed in the two connection design cases. Uniform over the height peak LFRS story drift equal 6 % and 1 % was observed due to EQ6 and EQ7, respectively. The residual LFRS story drift was also uniform over the height and equal to 2 % and almost zero due to EQ6 and EQ7, respectively.

The fact that the LFRS story drift is uniform over the height of the building model along with the fact that the LFRS story drift is not sensitive to the use of force-limiting connections indicates that the LFRS story drift is primarily controlled by the nonlinear inelastic response of the controlled rocking base mechanism. Fig. 14 shows the period of the first, second and third modes computed using the tangent stiffness at the end of each converged step of the nonlinear earthquake simulation of the connection design case RE due to EQ6 and EQ7. The upper plots include the periods of the first mode as computed (black line) and the periods of the first mode averaged within a one second moving time window (gray line). The bottom two plots exclude the as computed first mode periods and focus on a period range between 0 seconds and 20 seconds. Large variation of the first mode period is observed due to EQ6 and EQ7. The averaged first mode period range due to EQ6 during the duration of the pulse is between 2 seconds and 20 seconds. The averaged first mode period range due to EQ7 during the duration of the pulse is 1 second to 8 seconds. The variation in the second mode and third mode periods is less significant than the variation in the first mode period. The nonlinear inelastic force-displacement response of the force-limiting floor-to-LFRS connections, placed directly in the seismic load path, practically modifies the second (and higher) modal stiffness of the building model which results in the mode 2 period elongation. The modification of the second (and higher) mode dynamic characteristics of the building model allows for the limitation of the higher mode effects.

Fig. 15 shows the floor displacement spectra in the ninth floor, seventh floor, and second floor for RE and $R_{DC} = 2.0$ connection design cases due to EQ6 and EQ7. The ground motion spectral displacements are shown as reference. The ground spectral displacement for EQ6 is

large relative to EQ7, even for periods close to the first mode period of the SC-CBF model. As a result, significant nonlinearity is introduced at the controlled rocking base mechanism due to EQ6 associated with the relatively large period elongation. The first mode period was already oscillating around the five seconds period range at the beginning of the EQ6 pulse excitation leading to practically resonance of the elongated first mode period with the period of the pulse. This is the reason for the large amplitude LFRS story drift and the large floor spectral displacements. In case of EQ7 similar observations can be made with the exception that the magnitude of the velocity of the pulse was lower and the period elongation at the beginning of the pulse was smaller resulting to smaller LFRS story drift and floor displacement spectra compared to EQ7.

In summary, systems with nonlinear inelastic rocking base mechanism may not be suitable for seismic regions where ground motions with near-fault characteristics are excepted. The results of the present study indicate that this observation is independent of the use of force-limiting connections between the floors and the SC-CBF. A future study focusing on the effect of the near-fault ground motions on SC-CBFs with force-limiting connections may be needed.

7. Summary and conclusions

A systematic numerical study investigated the influence of force-limiting connections on the seismic response of a nine-story self-centering concentrically braced frame (SC-CBF) building subjected to design basis earthquake (DBE) ground motions with varying characteristics. A baseline SC-CBF model with rigid-elastic (RE) connection design is used for comparison. The effects of first mode and higher mode responses was discussed. Recommendations associated with the limiting forces used to design the force-limiting connections were provided. The conclusions from the analysis of the results derived from the numerical earthquake simulations are the following:

- **Mitigation of higher-mode effects:** Force-limiting connections, placed directly in the path of the seismic-induced horizontal inertial forces transferred from the floors to the LFRS, are highly effective in reducing the contribution of higher-mode responses to the acceleration and force responses of the building. As a result, a significant reduction in the magnitude and variability of the acceleration and force responses is possible.
- **Reduction in force and acceleration demands:** The use of force-limiting connections significantly reduces peak floor accelerations, brace axial forces, and connection forces compared to the baseline model with RE connections. These reductions help mitigate demands on both structural and acceleration-sensitive nonstructural components. The reductions in the connection forces increase the confidence in predicting the forces acting on the LFRS, and as a result, structural engineers can reliably use capacity design principles to design the braces, beams, and columns of the SC-CBFs. The reductions associated with the brace axial forces demonstrate that it is possible to reliably design the braces to remain linear elastic.
- **Reduced response variability:** Models with force-limiting connections exhibit reduced variability (dispersion) in acceleration and force seismic responses across the ground motion suite. This improved structural behavior enhances the predictability and reliability of the system's seismic performance. More specifically, the reduction in variability increases the confidence in predicting the floor total accelerations and force responses expected to develop due to ground motions with varying characteristics.
- **Comparable drift and shear performance:** Despite the changes in floor-to-LFRS connection force-displacement response, the story drifts and GLRS shear forces remain comparable between the force-limiting and RE connection models. This indicates that the first-mode dominant response continues to be governed primarily by the controlled rocking base mechanism. The mean residual story drift remained relatively low due to the self-centering capability of the concentrically braced steel frame.
- **Connection design recommendations:** The force-based design method can be used as a practical and effective process for determining the limiting forces F_{Lx}. A parametric study on the connection design forces shows that normalized seismic responses are minimized when R_{DC} is between 1.5 and 2.5. This range of R_{DC} provides reasonable estimate of F_{Lx} allowing limitation of the force and acceleration responses without increasing the drift responses.

Overall, force-limiting floor-to-LFRS connections can be used to enhance the resilience of multistory buildings with planar reinforced concrete walls, reinforced concrete core walls, reinforced concrete precast rocking walls, or rocking steel braced frames.

CRediT authorship contribution statement

Georgios Tsampras: Writing – review & editing, Writing – original draft, Visualization, Validation, Software, Resources, Project administration, Methodology, Investigation, Formal analysis, Data curation, Conceptualization; **Richard Sause:** Writing – review & editing, Supervision, Funding acquisition.

Data availability

Some or all data, models, or code that support the findings of this study are available from the corresponding author upon reasonable request. Experimental data from previous research conducted for the development of the force-limiting deformable connections and the development of the friction devices referenced in this paper are available at DesignSafe-CI [44,45].

Relevance to resilience

The well defined seismic load path in controlled rocking steel braced frames with floor-to-LFRS connections reduces both the magnitude and variability of force and acceleration seismic demands. Lower response magnitudes result in reduced structural and nonstructural damage and improved post-earthquake functionality. Reduced variability increases confidence in response predictions, design reliability, and the ability to meet target performance and resilience objectives associated with higher confidence in achieving accelerated post-earthquake functional recovery.

Declaration of interest

The authors declare that they have no known competing financial interests or personal relationships that could have appeared to influence the work reported in this paper.

Acknowledgement

The authors gratefully acknowledge the financial support provided by Lehigh University, the Advanced Technology for Large Structural Systems (ATLSS) Engineering Research Center, and the Department of Structural Engineering at the University of California, San Diego. The authors also sincerely thank Dr. Brent Chancellor for his valuable advice and guidance throughout the course of this work. The presented study is based on the work by a large research team led by Professor Robert B. Fleischman under the project "NEESR: Inertial Force-Limiting Floor Anchorage Systems for Seismic Resistant Building Structures" with the support of grants from the National Science Foundation, award no. CMMI-1135033 in the George E. Brown, Jr. Network for Earthquake Engineering Simulation Research (NEESR) program and award no. CMMI-0402490 for the George E. Brown, Jr. Network for Earthquake Engineering Simulation (NEES) consortium operations. Any opinions, findings, and conclusions expressed in this paper are solely those of the authors

and do not necessarily reflect the views of the individuals or institutions acknowledged above.

References

[1] Chen K, Tsampras G, Lee K., Structural connection with predetermined discrete variable friction forces 2023;2(1),1–17. https://linkinghub.elsevier.com/retrieve/pii/S2772741623000066.

[2] Zhong C, Christopoulos C., Self-centering seismic-resistant structures: historical overview and state-of-the-art 87552930211057581, 2021. https://doi.org/10.1177/87552930211057581. SAGE Publications Ltd STM

[3] Chancellor NB, Eatherton MR, Roke DA, Akbaş T., Self-centering seismic lateral force resisting systems: high performance structures for the city of tomorrow 2014;4(3), 520–48. Multidisciplinary Digital Publishing Institute; https://www.mdpi.com/2075-5309/4/3/520.

[4] Froozanfar M, Moradi S, Kianoush R, Speicher MS, Di Sarno L., Review of self-centering rocking systems for earthquake-resistant building structures: state of the art 2024;84:108607. https://doi.org/10.1016/j.jobe.2024.108607.

[5] Sause R, RiclesJ, Roke D, Seo C-Y, LeeKS., Design of self-centering steel concentrically-braced frames. In: US-Taiwan workshop on self-centering structural systems 2006 NCREE 2006; https://www.ncree.org/GetFile.ashx?id=10000616.

[6] Deierlein G, Billington S, Krawinkler H, Hajjar JF, Ma X, Borcher E, et al., Controlled rocking of steel-framed buildings with replaceable energy dissipating fuses. In: US-Taiwan workshop on self-centering structural systems 2006 NCREE, 2006.

[7] Gonner N., Design and experimental setup for self-centering steel concentrically braced frame test structure Lehigh University 2009; ISBN 978-1-109-12194-0. Google-Books-ID: 6n2TswEACAAJ.

[8] Roke DA., Damage-free seismic-resistant self-centering concentrically-braced frames Lehigh University 2010; ISBN 978-1-124-19539-1.

[9] Sause R, Ricles JM, Roke DA, Chancellor NB, Gonner NP., Large-scale experimental studies of damage-free self-centering concentrically-braced frame under seismic loading. In: Structures Congress 2010, American society of civil engineers. ISBN 978-0-7844-1130-8 2010; p. 1498–509. http://ascelibrary.org/doi/10.1061/41130%28369%29136.

[10] Sause R, Ricles JM, Roke DA, Chancellor NB, Gonner NP., Seismic performance of a slf-centering rocking concentrically-braced frame. In: Proceedings of the 9th US national and 10th Canadian conference on earthquake engineering, 2010. .

[11] Chancellor B, Seismic design and performance of self-centering concentrically-braced frames lehigh preserve Lehigh University 2014; ISBN 978-1-124-19539-1. https://preserve.lib.lehigh.edu/islandora/object/preserve3Abp-7266976.

[12] Chancellor B, Sause R, Ricles J, Tahmasebi E, Akbas T., Seismic response of post-tensioned steel rocking concentrically braced frames with various aspects ratios. In: Proceedings of the 4th International conference on computational methods in structural dynamics and earthquake engineering (COMPDYN 2013) institute of structural analysis and antiseismic research school of civil engineering national technical university of Athens (NTUA) Greece, 2013. ISBN 978-960-99994-2-7; p. 2866–79. https://doi.org/10.7712/120113.4708.C1290

[13] Eatherton MR, Ma X, Krawinkler H, Mar D, Billington S, Hajjar JF, et al., Design concepts for controlled rocking of self-centering steel-braced frames, 2014;140(11):04014082. . American Society of Civil Engineers. https://ascelibrary.org/doi/10.1061/%28ASCE%29ST.1943-541X.0001047.

[14] Christopoulos C, Zhong C., Towards understanding, estimating and mitigating higher-mode effects for more resilient tall buildings, 2022, 1(1):53–64. https://www.sciencedirect.com/science/article/pii/S2772741622000047.

[15] Wiebe L, Christopoulos C., Mitigation of higher mode effects in base-rocking systems by using multiple rocking sections 2009; 13:83–108. ZSCC: 0000101 tex.ids= wiebeMitigationHigherMode2009aTaylor & Francis. https://doi.org/10.1080/13632460902813315.

[16] Wiebe L, Christopoulos C, Tremblay R, Leclerc M., Mechanisms to limit higher mode effects in a controlled rocking steel frame. 2: large-amplitude shake table testing 2013;42(7):1069–86. tex.ids= wiebeMechanismsLimitHigher2013d. https://doi.org/10.1002/eqe.2258

[17] Wiebe L, Christopoulos C, Tremblay R, Leclerc M., Mechanisms to limit higher mode effects in a controlled rocking steel frame. 1: concept, modelling, and low-amplitude shake table testing: mechanisms to limit higher mode effects: concept, low-amplitude tests, 2013;42(7):1053–68. . ZSCC: NoCitationData[s0] tex.ids= wiebeMechanismsLimitHigher2013b, wiebeMechanismsLimitHigher2013c. https://doi.org/10.1002/eqe.2259

[18] Fleischman R, Restrepo J, Nema A, Zhang D, Shakya U, Zhang Z, et al., Inertial force-limiting anchorage system for seismic resistant building structures, 2015. In: Structures Congress Structures Congress. ISBN 978-0-7844-7911-7, p. 1302–13. https://doi.org/10.1061/9780784479117.111

[19] Tsampras G., Force-limiting floor diaphragm connection for earthquake-resistant buildings Lehigh University, 2016; ISBN 978-1-124-19539-1. https://preserve.lehigh.edu/etd/2851.

[20] Tsampras G, Sause R, Fleischman RB, Restrepo JI., An earthquake-resistant building system to reduce floor accelerations, 2015 In: 2015 NZSEE conference. ,.

[21] Tsampras G, Sause R, Fleischman RB, Restrepo JI, Zhang D., Deformable connection for eartquake-resistant building systems, 2015. In: 2015 JAEE international symposium on earthquake engineering, p. 8.

[22] Tsampras G, Sause R, Zhang D, Fleischman RB, Restrepo JI, Mar D, et al., Development of deformable connection for earthquake-resistant buildings to reduce floor accelerations and force responses, 2016;45(9):1473–94. tex.ids= tsamprasDevelopmentDeformableConnection2016. https://doi.org/10.1002/eqe.2718

[23] Tsampras G, Sause R, Fleischman RB, Restrepo JI., Experimental study of deformable connection consisting of buckling-restrained brace and rubber bearings to connect floor system to lateral force resisting system, 2017;46(8):1287–305. ZSCC: NoCitationData[s0] tex.ids= tsamprasExperimentalStudyDeformable2017. https://doi.org/10.1002/eqe.2856

[24] Tsampras G, Sause R, Fleischman RB, Restrepo JI., Experimental study of deformable connection consisting of friction device and rubber bearings to connect floor system to lateral force resisting system, 2018;47(4):1032–53. ZSCC: 0000008 tex.ids= tsamprasExperimentalStudyDeformable2018. https://doi.org/10.1002/eqe.3004

[25] Zhang Z, Fleischman RB, Restrepo JI, Guerrini G, Nema A, Zhang D, et al., Shake-table test performance of an inertial force-limiting floor anchorage system, 2018;47(10):1987–2011. ZSCC: 0000010 tex.ids= zhangShaketableTestPerformance2018 . https://doi.org/10.1002/eqe.3047

[26] Tsampras G, Sause R, Fleischman RB, Restrepo JI, Nema A, Zhang Z., Practical force-limiting deformable connections in buildings with rocking base mechanism and limited higher-mode responses. In: 12th national conference on earthquake engineering EERI, 2022.

[27] Mayorga CF, Tsampras G., Reinforced concrete wall buildings with force-limiting connections: modeling effects and uncertainty propagation, 2024; 53(4):1465–91. https://doi.org/10.1002/eqe.4073

[28] Tsampras G, Sause R., Practical design of force-limiting connections for buildings with reduced higher-mode responses 2024.

[29] Lee K, Tsampras G, Mayorga CF., Reinforced concrete core wall buildings with modified friction-based force-limiting connections: connection design considerations and 3d response to bidirectional ground motions, 2025; 151(2):04024203. tex.ids= leeReinforcedConcreteCore2025 publisher: American Society of Civil Engineers. https://doi.org/10.1061/JSENDH.STENG-13609

[30] Tsampras G, Sause R., Force-based design method for force-limiting deformable connections in earthquake-resistant buildings, 2022; 148(10). https://doi.org/10.1061/(ASCE)ST.1943-541X.0003456

[31] Fema NEHRP., recommended seismic provisions for new buildings and other structures. Lehigh University, 2015; ISBN 978-1-124-19539-1. https://www.fema.gov/sites/default/files/2020-07/fema_nehrp-seismic-provisions-new-buildings_p-1050-1_2015.pdf.

[32] McKenna F, Scott MH, Fenves GL., Nonlinear finite-element analysis software architecture using object composition, 2010; 24(1):95–107. American Society of Civil Engineers. https://doi.org/10.1061/(ASCE)CP.1943-5487.0000002

[33] Fema., Quantification of building seismic performance factors, 2009.

[34] PEER., PEER ground motion database, 2005, https://ngawest2.berkeley.edu/.

[35] American Society of Civil Engineers., Minimum design loads and associated criteria for buildings and other structures American society of civil engineers, 2022; 7 ed. ISBN 978-0-7844-1578-8 978-0-7844-8349-7. https://doi.org/10.1061/9780784415788

[36] Baker JW., Conditional mean spectrum: tool for ground-motion selection, 2011;137(3):322–31. American Society of Civil Engineers. https://doi.org/10.1061/(ASCE)ST.1943-541X.0000215

[37] Shome N, Cornell CA, Bazzurro P, Carballo JE., Earthquakes, records, and nonlinear responses, 1998; 14(3):469–500. SAGE Publications Ltd STM. https://doi.org/10.1193/1.1586011.

[38] Luco N, Cornell CA., Structure-specific scalar intensity measures for near-source and ordinary earthquake ground motions, 2007; 23(2):357–92. Publisher: SAGE Publications Ltd STM. https://doi.org/10.1193/1.2723158.

[39] Iervolino I, Cornell CA., Record selection for nonlinear seismic analysis of structures, 2005; 21(3):685–713. Publisher: SAGE Publications Ltd STM. https://doi.org/10.1193/1.1990199.

[40] Kafali C, Grigoriu M., Seismic fragility analysis: application to simple linear and nonlinear systems, 2007; 36(13):1885–900. https://doi.org/10.1002/eqe.726

[41] Grigoriu M., To scale or not to scale seismic ground-acceleration records, 2011; 137(4):284–93. Publisher: American Society of Civil Engineers. https://doi.org/10.1061/(ASCE)EM.1943-7889.0000226

[42] Mayorga CF, Tsampras G, Bocchini P, Mursel S., Overview of a project on resilience-based design of buildings with accelerated post-earthquake functional recovery. In: 18th U.S.-Japan-New Zealand workshop on the improvement of structural engineering and resilience ATC, 2024.

[43] Mavroeidis GP, Papageorgiou AS., A mathematical representation of near-fault ground motions, 2003;93(3):1099–131. https://doi.org/10.1785/0120020100

[44] Tsampras G, Sause R., Full-scale, components test of inertial force-limiting floor anchorage systems for seismic resistant building structures using a buckling restrained brace and steel reinforced low damping rubber bearings, 2016,. https://doi.org/10.4231/D3N87311M

[45] Fleischman R, Restrepo J, Sause R, Zhang D, Tsampras G, Zhang Z, et al., Half scale shake table test of a 4 story reinforced concrete building with eccentric shear walls, 2016. https://doi.org/10.4231/D39W0908G